Starnote 370
October 1998

Particle correlations as seen by the STAR detector

B. Erazmus, R. Lednický[1], P. Leszczyński[2], V. Lyuboshitz[3], L. Martin, T. Pawlak[2], J. Pluta[2], C. Roy, Yu. Sinyukov[4], A. Stavinsky[5], K. Werner
Laboratoire SUBATECH, Université de Nantes / Ecole des Mines de Nantes / IN2P3/CNRS, 4 rue Alfred Kastler, La Chantrerie, 44070 Nantes Cedex 03, France

Abstract

The ability of the STAR detector for determination of the space-time characteristics of particle production in heavy-ion collisions at RHIC from measurements of the correlation functions of identical and non-identical particles at small relative velocities is discussed. The possibility to use the correlations of non-identical particles for a direct determination of the delays in emission at time scales as small as 10^{-23} s is demonstrated. The influence of the multi-boson effects on pion multiplicities, single-pion spectra and two-pion correlation functions is discussed.

1 Introduction

The correlation function of particles with nearby velocities is sensitive to the relative space-time distances between the emission points due to the effects of Bose-Einstein or Fermi-Dirac statistics [1, 2, 3] and the strong and Coulomb final state interactions [4, 5, 6]

It should be emphasized that, depending on the characteristic space-time distance between particle emission points, both Coulomb and nuclear final state interactions can significantly influence the shape of the correlation function of identical particles (e.g., they dominate in case of two-proton correlations) and they are the main source of correlations of non-identical particles [6]-[8]. In particular, the shape of the correlation function of two charged particles (identical or non-identical) emitted at large relative distances in their c.m.s. is mainly determined by the Coulomb interaction and is increasingly sensitive to this distance with increasing particle masses and charges, i.e. with decreasing Bohr radius of the particle pair (see Section 6).

Particle correlations at high energies usually measure only a small part of the space-time emission volume since, due to substantially limited decay momenta of few hundred MeV/c, the sources, despite their fast longitudinal motion, emit the correlated particles with nearby velocities mainly at nearby space-time points. The dynamical examples are sources-resonances [9]-[15], colour strings [16, 17], hydrodynamical expansion [18]-[25].

[1]Permanent address: Institute of Physics, Na Slovance 2, 18040 Prague 8, Czech Republic
[2]Permanent address: Institute of Physics, Warsaw University of Technology, Koszykowa 75, 00-662 Warsaw, Poland
[3]Permanent address: JINR Dubna, P.O.Box 79, Moscow, Russia
[4]Permanent address: Institute for Theoretical Physics of National Acad. Sci., Kiev 252143, Ukraine
[5]Permanent address: ITEP, B. Cheremushkinskaya 25, 117259 Moscow, Russia

Thus, the features of emitting sources can be investigated in the frame of an approach which includes the dynamics of the emission process as well as the effects of quantum statistics (QS) and final state interactions (FSI) (see Section 2). Different mechanisms are considered in theoretical models: string and colour rope formation, hydrodynamical expansion, resonance production, rescattering, mean field effects etc., and finally the deconfinement transition and the creation of quark-gluon plasma (QGP). It is important, that particle correlations contain the information about the dynamical evolution of the emission process, such as proper time of decoupling (freeze-out), duration of particle emission and the presence of collective flows. In particular, the decoupling time and intensity of transversal flows should be closely related to the QGP formation and to the latent heat of the phase transition [18, 20, 22].

The identical-particle interferometry yields an important information on the relative space-time distances between the emission points of the particles of given type. Under certain conditions this relative information can be transformed to the absolute one, such as the decoupling proper time in the case of an expansion process. Measuring the decoupling times for various particle species and assuming the one and the same onset time for all emission processes, we can even estimate the possible delays in the emission of different particles. On the other hand, the correlations of non-identical particles appear to be directly sensitive to the delays in particle emission and thus can serve as a new source of the important complementary information to the standard interferometry measurements.

Thus the directional analysis of the correlations of two non-identical particles, in contrast to the identical ones, allows to measure not only the anisotropy of the distribution of the relative space-time coordinates of the emission points, but also - its asymmetry [8]. In particular, the differences in the mean emission times of various particle species can be directly determined, including their signs (see Section 3 and 6). This opens a new possibility to determine, in a model independent way, which sort of particles ($K^+, K^-, \pi^+, \pi^-, p...$) was emitted earlier and which later at very short time scales of several fm/c or higher. In particular, this effect could be useful to indicate the formation of QGP. Note that usually kaons are expected to be emitted earlier than pions due to their larger mean free path. In the case of strangeness distillation from the mixed hadronic and QGP phase a delay is expected between the emission of strange and antistrange particles.

As far as methodical problems are concerned, the correlation function of non-identical particles, contrary to the case of identical pairs, is practically not influenced by the two-track resolution. The influence of the momentum resolution is expected to be similar as in the case of identical-particle interferometry and it should be studied in detail for various particle pairs (see Section 6).

Correlations between particles with nearby velocities are usually considered in the limit of a low phase-space density such that the possible multi-particle effects can be neglected. This approximation seems to be justified by present experimental data which does not point to any spectacular multi-particle effects neither in single-particle spectra nor in two-particle correlations. Nevertheless, these effects can be of some importance for realistic simulations of heavy-ion collisions [26] or they can clearly show up in some rare events or the regions of momentum space in which the pion phase-space density becomes large (see [27] and Section 4). Provided that the space-time characteristics of slow pion emission are similar as in the whole range of p_t, the phase-space density becomes larger for smallest transverse momenta $p_t < 0.2GeV/c$ and could result in remarkable multi-boson effects. In the region of the smallest transverse momenta, $p_t < 0.2GeV/c$, the STAR resolution is limited by the SVT and SSD resolution capabilities. This momentum region, in which the identification of particles and the determination of their momenta is very difficult, is treated separately in our analysis.

The single-event interferometry appears quite realistic not only at LHC but also at RHIC energies though the value of dn/dy expected at STAR, being of the order of 10^3, is by a factor of 10 - and the number of pion pairs by a factor of 10^2 - smaller than at LHC. One should take into account, however, that the number of pairs contributing to the interference effect is proportional to the inverse interference volume. At AGS and SPS energies the interference volume seems to scale with dn/dy. Thus a factor of 10 is likely to be compensated for due to smaller interference volume at RHIC. Since further the effect of Coulomb repulsion eats a smaller part of the interference peak at RHIC, the net suppression with respect to LHC will be probably less than one order in magnitude only. Since most of the pions contributing to the interference effect are emitted with low transverse momenta, the possibility of the single-event interferometry will strongly rely on the particle identification and momentum measurement in this special region.

In present paper we focus on correlations of particles at small relative momenta. Correlations at large relative momenta are also of interest at STAR. Moreover some special class of the latter is expected to be particularly interesting at RHIC compared with SPS and LHC. An example are the azimuthal correlations expected between heavy baryons and antibaryons (open charm and anticharm particles) due to momentum conservation in the local interaction producing such pairs. Those correlations will be observed in standard hadron processes but should be destroyed completely in the case of QGP formation. To get reliable the cross section for the process of the heavy-particles production one should study high-energy interactions. However, the corresponding large particle multiplicities result in decreasing of the azimuthal correlation itself. So there is some optimum in initial energy which seems to be close to the RHIC region.

2 General formalism

As usual we assume sufficiently small phase-space density of the produced multi-particle system, such that the correlation of two particles emitted with a small relative velocity in nearby space-time points is influenced by the effects of their mutual QS and FSI only. The ideal correlation function $R(p_1,p_2)$ of the two particles is defined as a ratio of their differential production cross section to the reference one which would be observed in the absence of the effects of QS and FSI. For light mesons and baryons produced in heavy ion collisions or at sufficiently high energies, we can neglect kinematic constraints and most of the dynamical correlations and construct the reference distribution, e.g., with the help of particles from different events.

Assuming the momentum dependence of the one-particle emission probabilities inessential when varying the particle 4-momenta p_1 and p_2 by the amount characteristic for the correlation due to QS and FSI, i.e. assuming that the components of the mean space-time distance between particle sources are much larger than those of the space-time extent of the sources, we get the well-known result of Kopylov and Podgoretsky for identical particles, modified by the substitution of the plane wave $e^{ip_1x_1+ip_2x_2}$ by the non-symmetrized Bethe-Salpeter amplitudes in the continuous spectrum of the two-particle states $\psi^{S(+)}_{p_1p_2}(x_1,x_2)$ [6]. For non-identical particles

$$R(p_1,p_2)=\sum_S \rho_S\langle|\psi^{S(+)}_{p_1p_2}(x_1,x_2)|^2\rangle_S, \tag{1}$$

where the averaging should be done over the 4-coordinates $x_i=\{t_i,\mathbf{r}_i\}$ of the emission points of the two particles in a state with total spin S, populated with the probability ρ_S, $\sum_S \rho_S = 1$:

$$\langle f\rangle_S=\int f\cdot D^S_2(p_1,x_1;p_2,x_2)\,d^4x_1\,d^4x_2/P^S_2(\mathbf{p}_1,\mathbf{p}_2). \tag{2}$$

Here the two-particle emission function D^S_2 is a non-equal time analog of the two-particle Wigner density and

$$P^S_2(\mathbf{p}_1,\mathbf{p}_2)=\int D^S_2(p_1,x_1;p_2,x_2)\,d^4x_1\,d^4x_2 \tag{3}$$

is the normalized to unity momentum distribution of the two uncorrelated (non-interacting) particles. For identical particles, the Bethe-Salpeter amplitude in Eq. (1) should be properly symmetrized:

$$\psi^{S(+)}_{p_1p_2}(x_1,x_2)\to[\psi^{S(+)}_{p_1p_2}(x_1,x_2)+(-1)^S\psi^{S(+)}_{p_2p_1}(x_1,x_2)]/\sqrt{2}. \tag{4}$$

After the separation of the two-particle c.m.s. motion: $\psi^{S(+)}_{p_1p_2}(x_1,x_2)=e^{iPX}\psi^{S(+)}_{\tilde{q}}(x)$, where $X=[(p_1P)x_1+(p_2P)x_2]/P^2$ and $P\equiv 2p=p_1+p_2$ are the pair c.m.s. 4-coordinate and its 4-momentum respectively, the Bethe-Salpeter amplitude in Eq. (1) can be substituted by the amplitude $\psi^{S(+)}_{\tilde{q}}(x)$, depending only on the relative 4-coordinate $x\equiv\{t,\mathbf{r}\}=x_1-x_2$ and the generalized relative 4-momentum $\tilde{q}=q-p(qp)/p^2$, $q=p_1-p_2$. In the two-particle c.m.s. $\mathbf{p}^*_1=-\mathbf{p}^*_2\equiv\mathbf{k}^*$, $\tilde{\mathbf{q}}^*=2\mathbf{k}^*$, $\tilde{q}^*_0=0$. At equal emission times in the two-particle c.m.s. ($t^*=t^*_1-t^*_2=0$) this amplitude coincides with a stationary solution of the scattering problem $\psi^{S(+)}_{-\mathbf{k}^*}(\mathbf{r}^*)$, having at large r^* the asymptotic form of a superposition of the plane and outgoing spherical waves. It can be shown [6] that the amplitude $\psi^{S(+)}_{\tilde{q}}(x)$ can usually be substituted by this solution (*equal time* approximation).

Note that the two–particle correlations are often analyzed in terms of the *out* (x), *side* (y) and *longitudinal* (z) components of the vector $\mathbf{Q}=\{Q_x,Q_y,Q_z\}\equiv 2\mathbf{k}^*$ or - the invariant variable $Q_{inv}=|\mathbf{Q}|\equiv 2k^*$. Here the *out* and *side* denote the transverse, with respect to the reaction axis, components of the vector $\mathbf{Q}$, the *out* direction is parallel to the transverse component of the pair momentum $\mathbf{P}$. Sometimes, to get rid of a fast longitudinal motion of the particle sources, the longitudinally comoving system (LCMS) is introduced. In this system $P_z=0$ so that the vectors $\mathbf{q}$ and $\mathbf{Q}$ coincide except for the component $q_x=\gamma_\perp Q_x$, where $\gamma_\perp$ is the LCMS Lorentz factor of the pair.

3 Measurements of the delays in particle emission

The correlation function of two non-identical particles, compared with the identical ones, contains a principally new piece of information on the relative space-time asymmetries in particle emission [8]. In particular, it allows for a measurement of the mean relative delays $\langle t_1 - t_2 \rangle$ in particle emission. This is clearly seen in the case of neutral particles when the two-particle amplitude $\psi^{S(+)}_{-\mathbf{k}^*}(\mathbf{r}^*)$ takes on the form

$$\psi^{S(+)}_{-\mathbf{k}^*}(\mathbf{r}^*) = e^{-i\mathbf{k}^*\mathbf{r}^*} + \phi^S_{k^*}(r^*). \tag{5}$$

Here the scattered wave $\phi^S_{k^*}(r^*)$ is practically independent of the directions of the vectors $\mathbf{k}^*$ and $\mathbf{r}^*$ since we consider sufficiently small momenta k^* of the particles in their c.m.s. so that their interaction is dominated by s-waves. The correlation function in the form

$$\begin{aligned} R(p_1,p_2) &= \sum_S \rho_S \langle |\psi^{S(+)}_{-\mathbf{k}^*}(\mathbf{r}^*)|^2 \rangle_S \\ &= 1 + \sum_S \rho_S \langle |\phi^S_{k^*}(r^*)|^2 + 2\mathrm{Re}\phi^S_{k^*}(r^*)\cos\mathbf{k}^*\mathbf{r}^* - 2\mathrm{Im}\phi^S_{k^*}(r^*)\sin\mathbf{k}^*\mathbf{r}^* \rangle_S \end{aligned} \tag{6}$$

is sensitive to the relative space-time asymmetry due to the odd term $\sim \sin\mathbf{k}^*\mathbf{r}^*$. Particularly, it allows for a measurement of the mean relative delays $< t > \equiv < t_1 - t_2 >$ in particle emission. To see this, let us make the Lorentz transformation from the rest frame of the source to the c.m.s. of the two particles: $r^*_L = \gamma(r_L - vt), r^*_T = r_T$. Considering, for simplicity, the behavior of the vector $\mathbf{r}^*$ in the limit $|vt| >> r$, we see that this vector is only slightly affected by averaging over the spatial distance $r << |vt|$ of the emission points in the rest frame of the source so that $\mathbf{r}^* \approx -\gamma\mathbf{v}t$. Therefore, the vector $\mathbf{r}^*$ is nearly parallel or antiparallel to the velocity vector $\mathbf{v}$ of the pair, depending on the sign of the time difference $t \equiv \Delta t = t_1 - t_2$. The sensitivity to this sign is transferred to the correlation function through the odd in $\mathbf{k}^*\mathbf{r}^* \approx -\gamma\mathbf{k}^*\mathbf{v}t$ term provided the sign of the scalar product $\mathbf{k}^*\mathbf{v}$ is fixed.

For charged particles there arise additional odd terms due to the confluent hypergeometrical function $F(\alpha,1,z) = 1 + \alpha z/1!^2 + \alpha(\alpha+1)z^2/2!^2 + \ldots$ modifying the plane wave in Eq. (5):

$$\psi^{S(+)}_{-\mathbf{k}^*}(\mathbf{r}^*) = e^{i\delta}\sqrt{A_c(\eta)}[e^{-i\mathbf{k}^*\mathbf{r}^*}F(-i\eta,1,i\rho) + \phi^S_{ck^*}(r^*)], \tag{7}$$

where $\rho = \mathbf{k}^*\mathbf{r}^* + k^*r^*$, $\eta = (k^*a)^{-1}$, $\delta = \arg\Gamma(1+i\eta)$ is the Coulomb s-wave phase shift, $A_c(\eta) = 2\pi\eta/[\exp(2\pi\eta) - 1]$ is the Coulomb penetration factor (sometimes called Gamow factor) and a is the Bohr radius of the two-particle system. Clearly, at a given distance r^*, the effect of the odd component in the Coulomb wave function is of increasing importance with a decreasing Bohr radius of the particle pair, i.e. for particles of greater masses or electric charges.

It is clear that in the case of a dominant time asymmetry, $v\langle |t| \rangle \gg \langle r \rangle$, a straightforward way to determine the mean time difference $\langle t \rangle$ is to measure the correlation functions $R_+(\mathbf{k}^*\mathbf{v} \geq 0)$ and $R_-(\mathbf{k}^*\mathbf{v} < 0)$ (see Fig. 23). Depending on the sign of $\langle t \rangle$, their ratio R_+/R_- should show a peak or a dip in the region of small k^* and approach 1 at large values of k^* [6]. As the sign of the scalar product $\mathbf{k}^*\mathbf{v}$ is practically equal to that of the difference of particle velocities $v_1 - v_2$ (this equality is always valid for particles of equal masses), the sensitivity of the correlation functions R_+ and R_- to the sign of the difference of particle emission times has a simple explanation in terms of the classical trajectory approach (see, e.g., [28]). Clearly, the interaction between the particles in the case of an earlier emission of the faster particle will be weaker compared with the case of its later emission (the interaction time being longer in the latter case leading to a stronger correlation). It

[6] In the absence of the Coulomb interaction this ratio approaches 1 also at $k^* \to 0$.

means that $|R_+ - 1| < |R_- - 1|$ provided that $\langle t_1 - t_2\rangle < 0$. In particular, in the case of negligible contribution of the strong FSI, when $(R-1)$ is positive\negative for the pairs of particles with unlike\like-sign charges, we may expect that, at $\langle t_1 - t_2\rangle < 0$, the ratio R_+/R_- is lower\higher than unity. Noting that the Bohr "radius" a is negative\positive for the pairs of particles with unlike\like-sign charges, this expectation is in accordance with Eqs. (1) and (7) at $k^* \to 0$, $\langle r^*\rangle \ll |a|$ and $\langle|\phi^S_{ck^*}(r^*)|\rangle \ll 1$. Indeed, taking into account that for the pairs of uncorrelated particles at $k^* \to 0$ the distribution of the vector $\mathbf{k}^*$ approaches the isotropic one,

$$R_+/R_- \approx 1 + 2\frac{\langle r_L^*\rangle}{a} \to 1 - 2\frac{\langle \gamma v(t_1 - t_2)\rangle}{a}, \tag{8}$$

where the arrow indicates the limit $v\langle|t|\rangle \gg \langle r\rangle$.

For practical applications of the method it may be useful to note that the pairs characterized by a small value of the scalar product $\mathbf{k}^*\mathbf{v} = k^* v\cos\psi$ are not sensitive to the asymmetry $\langle r_L^*\rangle$ and to the related mean difference of the emission times $\langle\Delta t\rangle$. Therefore, the method sensitivity can be increased by rejecting the pairs with a small value of $|\cos\psi|$. The optimum cut $|\cos\psi| > 1/3$ corresponds to the enhancement factor $\sqrt{32/27} \doteq 1.09$ in the method sensitivity which is defined as a ratio of the effect to its error. The maximal sensitivity enhancement factor of $\sqrt{4/3} \doteq 1.16$ (35% gain in the statistics) can be obtained by replacing the above sharp angular cut with a weight $|\cos\psi|$ for each pair [7].

4 Multi-boson effects

In future heavy-ion experiments at RHIC and LHC one expects to obtain thousands of pions per unit of rapidity. Since pions are bosons there can be multi-boson effects enhancing the production of pions with low relative momenta thus increasing the pion multiplicities, softening their spectra and modifying the correlation functions. One can even hope to observe new interesting phenomena like boson condensation or speckles in some rare events or certain kinematic regions with a large pion density in the 6-dimensional phase space: $f = (2\pi)^3 d^6n/d^3\mathbf{p}d^3\mathbf{x} >$, of the order of unity (see, e.g., [3],[29]-[35]).

In the low-density limit ($f \ll 1$), the mean phase-space density at a given momentum $\mathbf{p}$ can be estimated as the mean number of pions interfering with a pion of momentum $\mathbf{p}$ (rapidity y and transverse momentum $\mathbf{p}_t$) and building the Bose-Einstein (BE) enhancement in the two-pion correlation function [34, 35]: $\langle f\rangle_{\mathbf{p}} \sim \pi^{3/2}N(\mathbf{p})/V$, where $N(\mathbf{p}) = d^3n/d^3\mathbf{p}$ and $V = r_x r_y r_z$ is the interference volume defined in terms of the outward (r_x), sideward (r_y) and longitudinal (r_z) interferometric radii. Typically $\langle f\rangle_{\mathbf{p}} \sim 0.1$ for mid-rapidities and $p_t \sim \langle p_t\rangle$ [34]. The data are also consistent with the phase-space density of pions in local thermal equilibrium [36].

At AGS and SPS energies the interference volume V seems to scale with dn/dy (see, e.g., [37, 38]) pointing to the freeze-out of the pions at a constant phase-space density. If this trend survives up to the RHIC energies then there will be no spectacular multi-boson effects in the ordinary events even at STAR and the standard two-particle interferometry

[7] It is easy to check that the weight $|\cos\psi|^n$ enhances the method sensitivity by a factor of $(2n+1)^{1/2}/(n/2+1)$. The optimal value of $n = 1$ yields the enhancement factor equal to the maximal possible one, following from the moment or fitting method.

technique could be used to measure the space-time intervals between the production points.

The multi-boson effects can show up however in certain classes of events. Thus a strong transversal flow can lead to rather dense gas of soft pions in the central part of the hydrodynamical tube at the final expansion stage (see, e.g., [21]). Another reason can be the formation of quark-gluon plasma or mixed phase. Due to large gradients of temperature or velocity the hydrodynamical layer near the boundary with vacuum can decay at a large phase-space density and lead to pion speckles even at moderate transverse momenta [39].

Generally, the account of the multi-boson effects is extremely difficult task. Even on the neglection of particle interaction in the final state the requirement of the BE symmetrization leads to severe numerical problems which increase factorially with the number of produced bosons [30, 31]. In such a situation, it is important that there exists a simple analytically solvable model [32] allowing for a study of the characteristic features of the multi-boson systems under various conditions including those near the Bose condensation. This model assumes factorization of the multi-boson emission function in terms of the single-boson ones, the latter parametrized in a Gaussian form:

$$D(p,x) = \frac{1}{(2\pi r_0\Delta)^3}\exp(-\frac{\mathbf{p}^2}{2\Delta^2} - \frac{\mathbf{r}^2}{2r_0^2})\delta(t). \tag{9}$$

The original multiplicity distribution of the uncorrelated bosons is usually taken in a Poissonian form.

The multi-boson correlations lead to distortions of the original multiplicity distribution as well as single- and two-particle momentum distributions (increasing the original mean multiplicity), of the single-pion spectra (enhancing production of the pions with low p_t and small y) and, to a lesser extent, of the two-pion correlation functions (the correlation function at a given multiplicity becoming lower and wider). Such distortions are small in the case of interference of only two or three identical particles. However, they can become essential for the events with a large number of identical bosons due to factorially increasing number of the correction terms [30] (see also [3] and [32]). For the processes characterized by a high (> 0.1) phase-space density of the identical bosons at the freeze-out time the multi-boson effects can no more be considered as a correction [30].

This is demonstrated, for multiplicity distribution, in Figs. 1 and 2. Thus, at $r_0 = 2.1$ fm and $\Delta = 0.25$ GeV/c, the BE effect transforms the original Poissonian multiplicity distribution with $\eta = 30$ (dotted curve in Fig. 1a) to the one with much higher mean and dispersion values (solid line in Fig. 1a). It can be shown [27], using the Gaussian ansatz in Eq. 9, that with the increasing phase space density parameter

$$\xi = \eta/\beta, \quad \beta = (r_0\Delta + 1/2)^3, \tag{10}$$

the BE affected multiplicity distribution approaches the BE one $w_{BE}(n) = \nu^n/(1+\nu)^{n+1}$ with the mean multiplicity $\nu = \xi/(1+\xi)$.

The exponential tail expected for the BE distribution is clearly seen in Fig. 1b where the results are presented in logarithmic scale for $\eta = 10$, $\Delta = 0.25$ GeV/c and $r_0 = 1.5$ fm. The slope parameter b in the exponential fit $w(n) = \text{const}\cdot\exp(-bn)$ of this tail at large n should be only a function of the variable ξ: $b = -\ln(\xi)$, where $\xi = \eta/\beta$. Such a scaling is demonstrated in Fig. 2a for various values of η, Δ and r_0. Note that $\xi = 0.95$ and 0.72 for Figs. 1a and 1b, corresponding to $b = 0.02$ and 0.27, respectively [8].

The mean multiplicity can be approximated as

$$\langle n \rangle \doteq \left[1 + \tilde{\xi}_{\mathbf{p}}/2^3 + \cdots + \tilde{\xi}_{\mathbf{p}}{}^{n_t-1}/n_t{}^3\right] \eta + \xi^{n_t}\nu, \tag{11}$$

where $n_t = r_0\Delta$ and $\tilde{\xi} = \eta/(r_0\Delta)^3$. At large phase-space volumes, $(r_0\Delta)^3 \gg 1$, the two terms in Eq. (11) can be considered as contributions of the BE gas and BE condensate respectively. In Fig. 2c we demonstrate the approach of the mean multiplicity $\langle n \rangle$ to the limiting scaling value $\nu = \xi/(1-\xi)$, though only for ξ very close to the explosion point $\xi = 1$ ($\xi > 0.99$). Instead, in the region of $\xi < 0.9$ indicated by present experiments, we can see an approximate ξ-scaling of the ratio $\langle n \rangle/\eta$ (Fig. 2b).

Note that the approximate ξ-scaling gives a possibility to overcome technical problems with factorially large numbers at high multiplicities. Thus some quantities can be calculated at small or moderate values of η or n and then rescaled to a large one provided the density parameter $\xi = \eta/\beta$ or $\xi_n = n/\beta$ is kept the same.

Since, in the realistic event generators, the multi-boson effects can be accounted for only in the lowest order cumulant approximation [26], it is instructive to study the saturation of these effects with the increasing number N_{cum} of the contributing cumulants. In Fig.3 we show N_{cum}-dependence of the ratio $\langle n \rangle/\eta$ of the BE affected mean multiplicity to the original one for different values of the density parameter ξ. Thus at $\xi = 0.8$ this ratio saturates at $N_{cum} \sim 10$ ($\sim 40\%$ increase of $\langle n \rangle$). At $N_{cum} = 4$, representing a limit due to the numerical problems [26], the effect is underestimated by $\sim 25\%$ ($\langle n \rangle/\eta \approx 1.3$ instead of 1.4). The situation is more optimistic for lower densities. For example, at $\xi = 0.5$ the effect ($\sim 15\%$ increase of $\langle n \rangle$) practically saturates at $N_{cum} = 4$.

Let us now consider the BE effect on single-boson spectra and two-boson correlation functions. At sufficiently large momenta, when the local density $< f_n >_{\mathbf{p}}$ remains small even for large boson multiplicities, the single-boson spectrum for a given multiplicity n is dominated by the contribution $\beta_n P(\mathbf{p})$ of the original spectrum

$$P(\mathbf{p}) = (2\pi\Delta^2)^{-3/2} \exp(\mathbf{p}^2/2\Delta^2), \tag{12}$$

$\beta_n = n\omega_{n-1}/\omega_n$, where ω_n is the BE weight of the n-boson event. Otherwise, at large local densities, it is determined by the asymptotic large-density spectrum

$$N_n(\mathbf{p}) \to n \left(\frac{r_0}{\pi\Delta}\right)^{3/2} \exp\left(-\frac{r_0}{\Delta}\mathbf{p}^2\right) \equiv nP_c(\mathbf{p}), \tag{13}$$

Similarly, the inclusive single-boson spectrum at small local densities tends to $\eta P(\mathbf{p})$ and, at large ones, it approaches the asymptotic high-density spectrum:

$$N(\mathbf{p}) \to \langle n \rangle P_c(\mathbf{p}). \tag{14}$$

[8]At the explosion point $\xi = 1$ the tail of the multiplicity distribution becomes a constant ($b = 0$) so that the mean multiplicity $\langle n \rangle$ would go to infinity provided that there are no energy-momentum constraints. Note that the corresponding critical original mean multiplicity $\eta_{cr} = \beta \equiv (r_0\Delta + 1/2)^3$ is close but different from that given in Eq. (9) of ref. [32].

The transfer of the original spectrum to the high-density one is demonstrated for the inclusive distribution in Fig. 4a and, more clearly, for ξ closer to the explosion point $\xi = 1$, in Fig. 4b [9].

The inclusive single-boson spectrum can be approximated as

$$N(\mathbf{p}) \doteq \left[1 + \tilde{\xi}_{\mathbf{p}}/2^{3/2} + \cdots + \tilde{\xi}_{\mathbf{p}}{}^{n_t-1}/n_t{}^{3/2}\right] \eta P(\mathbf{p}) + \xi^{n_t} \nu P_c(\mathbf{p}), \qquad (15)$$

where $\tilde{\xi}_{\mathbf{p}} = (2\pi)^{3/2}\eta P(\mathbf{p})/r_0{}^3 \equiv \tilde{\xi}\exp(-\mathbf{p}^2/2\Delta^2)$. Clearly, for large phase-space volumes, $(r_0\Delta)^3 \gg 1$, the two terms in Eq. (15) can be interpreted as contributions of the BE gas and BE condensate respectively. In Fig. 4 we compare the inclusive single-boson spectra with the approximate formula (15). Though the calculations were done for not very large phase-space volumes a good agreement is obtained. Experimentally the effect of BE "condensate" was searched for at SPS CERN as a low-p_t enhancement, however, with rather uncertain results (see, e.g., [40]).

It follows from Eq. 15 that for sufficiently large ($n_t = r_0\Delta >> 1$) and not very dense ($\xi << 1$) systems, similarly to the ξ-scaling of $< n > /\eta$ (see Fig. 2b), the ratio $N(\mathbf{p})/[\eta P(\mathbf{p})]$ scales with the local density parameter $\tilde{\xi}_{\mathbf{p}}$. It appeares that analogical scaling takes place also at fixed multiplicity n.[10] In Fig. 5 we show the ratio of the single-particle spectrum at fixed n to the dominant large-p contribution $\beta_n P(\mathbf{p})$ of the original spectrum calculated at $\mathbf{p} = 0$ as a function of ξ_n for various multiplicities n. An approximate ξ_n-scaling is seen up to ξ_n of the order of unity. At larger ξ_n this ratio approaches the limit $(2r_0\Delta)^{3/2}\xi_n$ which no more scales with ξ_n (see the corresponding curves in Fig. 5b). What scales at large ξ_n is not the ratio of the two contributions but the ratio of their integrals, n/β_n the limiting value of which is just equal to $\xi_n = n/\beta$ (see the corresponding curves in Fig.5).

Regarding the two-boson correlation function, for given multiplicity n, its intercept $R_n(0)$ decreases and its width increases with the increasing n or decreasing momentum p, both corresponding to the increasing local density. The well known [30, 31, 32] lowering and widening of the correlation function with the increasing multiplicity is demonstrated, in the considered model, in Fig. 6. For fixed p $R_n(0) \to 2$ at small ξ_n, p limit and $R_n(0) \to 1$ at large ξ_n, p (Fig. 7). Again we see scaling violation at intermediate ξ.

In Fig. 7 we show the intercept as a function of the multiplicity n and the density parameter $\xi_{n,\mathbf{p}}$ for several values of the mean momentum: $p = 0$, 0.1, 0.2 and 0.4 GeV/c. As expected, the intercept is practically constant at low local densities (small n or high p). As condensate develops, the intercept sharply falls down. The sharpness of this drop is however less pronounced at higher momenta even if plotted as a function of the local density. Clearly, this lack of density scaling is related to a strong decrease of the condensate contribution with the increasing momentum. To demonstrate the possibility of the observation of the condensate effect for soft pions produced in high multiplicity events even at SPS or RHIC energies, in Fig. 7 we indicate by the arrows the intercept values corresponding to $\xi_n = 3\xi = 1.5$ ($n \approx 3\langle n\rangle$).

In the inclusive case corresponding to the original Poissonian multiplicity distribution, the correlation function intercept is equal to 2 for any pion momenta or the local densities

[9] These results agree with those obtained in refs. [32, 33] (see also [35, 26] and references therein) except for a wrong conclusion in [32] that the width of the narrow peak due to the BE "condensate" is of $1/r_0$.

[10] Due to the complicated n-dependence of the BE weights ω_n entering the particle spectra, there is no analog of the simple tailing approximation (15) in this case.

[27]. At large local densities the two-boson spectrum approaches twice the product of the single-boson ones so that the inclusive correlation function tends to the limiting value of 2 even at large relative momenta. The corresponding increase of the width of the correlation function with the increasing density parameter ξ is demonstrated in Fig. 8.

It can be shown that in case of a dominant BE condensate contribution the interferometric radius squared (defined as a low-$\mathbf{q}^2$ slope of the correlation function) tends to zero (as $(1-\xi)$) whatever large is the geometric size of the system. The effective radius squared (related to the inverse effective width squared) vanishes at large phase space densities much slower (as $1/|\ln(1-\xi)|$) (see Fig. 8).

It should be noted that we have assumed that the original Poissonian multiplicity distribution extends to any arbitrarily large number of bosons. In reality, however, this number is limited due to the finite available energy. It is therefore interesting to see how fast the semi-inclusive spectra approach the inclusive limit with the increasing number n_{max} of the included pions. In Fig. 9 we demonstrate the n_{max}-dependence of the semi-inclusive correlation functions for a fixed value of the density parameter $\xi = 0.95$ and, in Fig. 10 - the n_{max}-dependence of the correlation function intercepts for different ξ-values. We can see that the width of the semi-inclusive correlation function increases with the increasing n_{max}, while its intercept decreases at small n_{max}, reaching a minimum at $n_{max} \approx \langle n \rangle$, and then approaches the limiting value of 2 roughly as $\log n_{max}$. The inclusive behavior is practically saturated at a moderate number of the included pions $n_{max} \approx 5\langle n \rangle$, thus justifying the neglect of the energy-momentum constraints.

The results of the considered simple model should not be taken, however, too literally since:

a) in contradiction with the experimental indications on a constant freeze-out phase space density, in the model there is no correlation between the emission volume and pion multiplicity;

b) the static character of the model can be justified (neglecting the transverse expansion) in a limited rapidity region only. Thus the pions with a rapidity difference greater than about unity have to be considered as originating from different static sources. Generally, however, these sources are not spherically symmetric;

c) the inclusive spectra at sufficiently high mean multiplicity are dominated by the condensate contributions of high multiplicities in both extreme cases of very narrow or very wide multiplicity distributions (compared with the Poissonian one) of the originally uncorrelated bosons. Thus the intercept of 2 of the inclusive correlation function in the Poissonian case is likely to be a maximal one. Since the original multiplicity distribution is in fact wider than the Poissonian one (*e.g.*, due to the fluctuations of the mean multiplicity), we can expect the intercept less than 2 not only for the correlation functions at fixed multiplicities but also for the inclusive ones;

d) there can be large local density fluctuations (not present in the model) which can give rise to noticeable multi-boson effects even at a moderate value of the mean phase space density;

e) on the other hand, the multi-boson effects can be somewhat suppressed due to a possible violation of the factorization assumption or due to the lack of the reflection symmetry of the emission volume;

f) for identical charged pions, the BE effects are also suppressed due to the Coulomb repulsion. Since this repulsion is important only in a weakly populated region of very small relative momenta, the suppression of the global BE weights ω_n is rather small. For example, for ω_2 this suppression, being about $(ar_0\Delta^2)^{-1}$, is usually less than one per mill. The Coulomb distortion of the global multi-boson effects is therefore negligible in the rare gas limit. Nevertheless, since the Coulomb repulsion destroys the formation of the condensates made up from positive and negative pions in the disjoint phase space regions, it leads to noticeable differences between charged and neutral pions in dense systems. Particularly, we can expect a decrease of the charge-to-neutral multiplicity ratio with the increasing phase space density.

5 Coulomb screening

Because of large numbers of positive and negative pions produced in heavy ion collisions, one could also raise a question about importance of the Coulomb screening effects violating the standard two-body treatment of the correlations in the low density limit. There are however arguments showing that the screening will be of minor importance even at LHC [27] (see also [41]). Note that in the scenario with a constant phase-space density the corresponding Debye radius

$$r_D = [4\pi(\rho_+ + \rho_-)e^2/T]^{-1/2}, \tag{16}$$

where $e^2 = 1/137$ and $\rho_+ + \rho_-$ is the total density of charged pions in the configuration space, will be also constant, up to a weak energy dependence due to the temperature T. Assuming that pions with a rapidity difference greater than unity come from spatially disjoint regions of phase-space, we can put [27]

$$\rho_+ = \left(\frac{\lambda}{(2\pi)^3}\right)^{1/2} \frac{dn_+/dy}{V} = \frac{\sqrt{2}}{\sqrt{\lambda}\pi^2} T^3 \langle f_+ \rangle_y \tag{17}$$

and obtain $r_D \approx 15$ fm at $\langle f_+\rangle_y \approx 0.1$ and $T \approx 200$ MeV/c ($r_D \sim 1/T$). Thus at LHC energies we can expect the characteristic distances between the pion production points comparable or larger than the screening radius r_D leading to a suppression of the usual two-particle Coulomb effects. In fact, two charged pions produced at a distance $r^* > r_D$ start to feel their Coulomb field only after some time when the density decreases to a value corresponding to Debye radius smaller than r^*. During this time the vector of the relative distance between the pion emission points increases approximately by [27]

$$\Delta\mathbf{r}^* = \frac{\mathbf{k}^*}{T} V^{1/3} [\left(\frac{r^*}{r_D}\right)^{2/3} - 1]. \tag{18}$$

Substituting $\mathbf{r}^*$ by $\mathbf{r}^* + \Delta\mathbf{r}^*$ in the argument of the Coulomb wave function, we can see however that the suppression of the Coulomb effect can be substantial only in the region of large relative momenta $k^* > T$ where the correlations due to QS and FSI are already negligible.

6 Two-particle correlation functions

Our correlation analysis is based on the generation of Pb-Pb events at $\sqrt{s} = 200 \cdot A$ GeV by the VENUS (version 5.21) event generator [42, 43] followed by the calculation of the correlation function for the selected pairs of identical or non-identical particles. The events were generated without the phase of the particle rescatterings and droplet formation which normally lead to increase of the space-time characteristics of particle emission (but also to an impressive increase of the computing time). Instead, we introduce the scale factor changing these characteristics in a controlled way. It allows us to study the sensitivity of the STAR detector to particular correlation effects.

The correlation functions were calculated using the momentum vectors of the selected particles in the CMS. For each pair of identical or non-identical particles the relative coordinates of the emission points and the relative momenta were calculated in the pair rest frame and the relative coordinates of the emission points and the relative momenta were calculated in the pair rest frame and the corresponding weight (depending, in the usual two-body approximation, only on these quantities) was attributed including the effects of quantum statistics (for identical particles) as well as the final state (strong and Coulomb) interactions. In this way we have taken into account not only the effects of the relative motion of particles but also the velocity of the pair in the CMS.

The correlations were studied for three types of particles: pions, kaons, protons and for some combinations of them. Correlations of identical and non-identical particles are considered separately and their comparison is made as well. Two extreme classes of the space-time characteristics are considered. First, a direct output of the VENUS (string-phase) generation is considered. It gives rather underestimated sizes of the emission region. Second, these values are multiplied by the scale factor α. The results presented here were obtained for $\alpha = 3.0$. As an example, Fig. 11 shows the distributions of the space-time coordinates of the pion emission points (x,y,z,t) in one generated event. The mean value of the particle emission radius is about 5 fm and the time about 4 fm/c in the CMS. The scaled values are thus of the order of 15fm.

To analyse the influence of the detector resolution on the correlation functions we have taken into account the resolution of the STAR detector [44]. All detected particles are divided into three classes: first one includes the particles registered by all the detection chain SVT+SSD+TPC ($(0.05 < P_t < 2.50) GeV/c$). For this class of the transverse momentum the resolution is, first of all, determined by the high resolution of the TPC. We have assumed that the momenta of all particles with $p_t > 0.2 GeV/c$ were measured with the resolution $(\Delta(1/P_t)/(1/P_t)) = 0.9\%$. In the region of the smallest transverse momenta $p_t < 0.2 GeV/c$ the resolution is limited by the SVT and SSD resolution capabilities. The space-time characteristics of the emission of slow pion are shown in Fig. 12. The space characteristics are similar to those in the whole range of p_t; the mean value of the emission time is slightly higher. The amount of particles which do not reach the TPC is determined by the p_t distribution and illustrated in Fig.13 for pions, kaons and protons. In all considered cases the particle rapidity is limited to the interval $(-1 < Y < 1)$.

The class of particles with the smallest p_t is, for several reasons discussed earlier, especially interesting, but also very difficult from the point of view of the identification and momentum determination. This class is treated separately in our analysis. Two cases of particle detection are considered. In the first case the momentum resolution corresponds to that of the SVT alone $(\Delta(1/P_t)/(1/P_t)) = 15\%$. In the second case, which takes into account the improvement of the resolution by the SSD, the value of 10% is assumed.

This approach does not take into account the double-track resolution and the directional dependence (different resolution for different momentum components). In this note we consider only the correlation function in Q_{inv} when the directional dependences are not of the primary importance. The problem of double-track resolution is especially significant for the identical particles and for the largest dimensions of the emission region. This problem is addressed later on here and will be the subject of a separate note, together with the questions of directional dependences in particle interferometry. Such an analysis requires, however, a detailed description of the particle detection in different parts of the detector, pattern recognition, track matching etc.

6.1 Correlations of identical pions

Fig.14a presents the correlation function for the pairs of positive pions registered by the SVT+SSD+TPC detection system. Different features, important for the correlation analysis, are demonstrated by some characteristic curves. The correlation effect inferring from the quantum statistics alone is indicated by the full squares. The stars show the correlation function corrected by the so called "Gamow factor". The form of that factor is also shown separately by the open stars. The result of the complete calculation including the detailed description of the strong and Coulomb final state interactions and quantum statistics is shown by the full circles. The open circles present the results of the complete calculations with the effect of the STAR detector resolution accounted for as described above. Note also that the presented correlation functions for pions were constructed for a single generated event. It seems that single-event interferometry is quite realistic for pions at the RHIC energies.

In the case of pions and for relatively small sizes of the emission region the Gamow correction only slightly overestimates the expected form of the correlation function resulting from quantum statistics. This overestimation, determined by the ratio of the relative distance between the emission points in the two-pion rest frame to the two-pion Bohr radius, is small due to a large value of 388 fm of the latter. The correlation function which can be observed (complete calculation - full or open circles) differs strongly, however, from that expected by the BE statistics alone. The effect of experimental resolution diminishes slightly the maximum and is most important for the smallest values of the four-momentum differences.

Fig.14b presents the same dependences as Fig.14a but for pions with the values of p_t limited to the region of the SVT and SSD detection $(0.05 < P_t < 0.20) GeV/c$. The similar form of the correlation functions in Figs. 15a and 15b indicates that the sizes of the emission region of slow pions do not differ significantly (in the VENUS simulation) from those emitted in the whole p_t interval. Also the single event statistics of pion pairs is sufficient for the interferometry analysis. The resolution effects are, however, slightly stronger in this case. The correlation functions corresponding to the detection of pions by the SVT only are presented in the Fig.14c The influence of the detector resolution is most pronounced here (note open circles) making almost invisible the Coulomb suppression for the smallest values of Q_{inv} (full circles).

The analogous set of results has been obtained for the space-time distributions of emitted pions multiplied by the scale factor $\alpha = 3.0$. In this case the mean value of the CMS size of pion emission region is about 17fm. We consider it as an upper estimate of the pion source dimensions. The correlation effect seen in Fig.15a is limited to the significantly narrower interval of Q_{inv} as compared with Fig.14a. The Gamow correction is clearly unapplicable here. Also the experimental resolution diminishes considerably the observed correlation maximum.

Figs.15b and 15c present the possibilities of the STAR detector for the analysis of the correlation effects for slow pions. In both cases the form of correlation function is strongly affected by the resolution effects. It seems that the distortions observed for the detection by the SVT alone can hardly be corrected for without a significant influence of the systematic errors.

6.2 Correlations of identical kaons

Generated with the VENUS model space-time characteristics of the kaon emission do not differ essentially from those of pions. The quantum statistical effect is therefore similar. However, the shape of the correlation function obtained with the complete calculations is quite different due to different Coulomb and strong final state interactions. The Coulomb effect is determined by the Bohr radius which is much smaller for two-kaon system than for pions. This implies the increase of the Q_{inv} region, affected by the negative correlations, by a factor of 3.5. For the same reason the Gamow factor cannot be used for the correction of the observed correlation functions.

The analysys of the correlation effects for kaons has been made in the same way as for pions. In figures 17a, b, c the analogous correlation functions obtained with the scale factor $\alpha = 1.0$, are presented. The mean value of the kaon emission CMS size generated by the VENUS code is about 5 fm. The Gamow factor correction overestimates the correlation effects due to quantum statistics in the whole range of Q_{inv} which is displayed in the figure. The relative disagreement is even more important for the greater values of Q_{inv}. Also the influence of the detector resolution is more pronounced than for pions. This is related to a wider Coulomb suppression region in the two-kaon case. In the case of limited transverse momenta (Figs. 16b and c) the shape of correlation functions is affected by the resolution effects even stronger.

For the scale factor $\alpha = 3.0$ (Fig. 17) the narrow effect of BE statistics is practically cancelled out by the common effects of strong and Coulomb interactions. The Gamow correction fails completely. The influence of the detector resolution is important even in the case of kaons detected by the whole detection system. For the small kaon momenta the correlation effect is weakly visible in the case of SVT+SSD detection and practically disappears if only the SVT registration is present.

Fig.18 presents an attempt to the one-event kaon interferometry. This result is obtained for the whole detection system, the scale factor $\alpha = 1.0$ and with an increased width of the Q_{inv} bins. The correlation effect with the STAR resolution (open circles) is visible however. Keeping in mind a good possibility of the one-event pion interferometry, this relatively weak effect can still be useful for a consistent analysis of the fluctuation effects in the frame of one-event studies at STAR.

6.3 Two-proton correlations

The correlations of two fermions, represented here by two protons, are shown in Figs. 19 and 20 in the same way as for pions and kaons. The quantum-statistical correlation effect is negative in this case, the correlation function reaching the value of 0.5 for $Q_{inv} = 0$. The Gamov correction is inapplicable here due to a small Bohr radius of two protons (57 fm) and due to the fact that at $Q_{inv} > 20MeV/c$ the correlation effect for relatively small effective sizes is mainly determined by the strong interaction.

In case of small value of the scale factor, $\alpha = 1.0$, the correlation effect for the complete calculation has the form of a broad peak with the maximum at 40 MeV/c. It is the joint result of a positive correlation, due to the strong interaction, and negative one resulting from the Coulomb and quantum-statistical effects. The influence of experimental resolution is rather strong changing the shape of the correlation function essentially.

In case of $\alpha = 3.0$ the form of the complete correlation function changes strongly . The peak converts into a dip for the smallest Q_{inv} values. It demonstrates a high sensitivity of the two-proton correlation function to the size of the proton emission region. The narrow effect of negative correlations is however filled up due to the experimental resolution. A relatively small number of emitted protons precludes the possibility to analyze the proton-proton correlations in the single events.

6.4 Correlations of non-identical particles

The non-identical particle correlations can be used, in principle, for the determination of the space-time parameters of the emission process in a similar way as the identical ones using the sensitivity of the Coulomb and strong interaction effects to the space and time intervals of particle emission. The sensitivity of the correlation function to the size of the emission region is tested in Figs. 21a, b and c for different two-particle systems. Fig.21a presents the correlation functions for $\pi^+\pi^-$ pairs and for the two values of the scale factor: $\alpha = 1.0$ and $\alpha = 3.0$. First, one can notice that the Gamow factor corresponds fairly well to the results of the complete calculations for the sizes of the order of 6fm. It means that in this case the correlation effect is dominated by the size-independent part of the Coulomb interaction. Second, the clear sensitivity to the size can be observed in the regions of the small relative momenta indicating a possibility to extract the source sizes from the different-charge pion correlations. However, the identical-pion correlations are more sensitive to the changes of the emission sizes, particularly for the smaller sources.

In case of K^+K^- system, Fig.21b, the behaviour of the correlation function is more complicated due to a smaller Bohr radius and the interplay of Coulomb and strong interactions. The Gamow factor is thus in a full disagreement with the form of the complete correlation function. It seems that, in this case, it is more difficult to determine the source sizes from the form of the correlation function.

A more clear situation and a better size sensitivity appears for the K^+p system, Fig.21c. The negative correlations due to the Coulomb repulsion are well sensitive to the size in the considered size region. The detector resolution introduces some distortion in the region of the smallest Q_{inv} but the sensitivity extends to sufficiently great Q_{inv} values to be separated experimentally.

The important experimental difference between the identical and non-identical particle correlation measurements should be stressed here. For non-identical particles there is no problem with the double-track resolution, even for the smallest values of the relative momenta. In the case of particles with opposite charges the deviations due to magnetic field are in opposite directions. For the particles of the same charge but different masses the small relative momentum in pair rest frame corresponds to quite different absolute momenta in the laboratory. The trajectories of such particles are thus well separated.

6.5 Sequence of particle emission

As discussed in Section 3, the non-identical particle correlations contain information about the sequence of particle emission, Fig. 22. To demonstrate this, we have introduced a shift in the time of particle emission for a given type of particles and for different values of the scale factor α. All the presented results correspond to K^+K^- pairs.

Three values of the time shift were considered: $<\Delta t>= 10, 0, -5 fm$ (Fig.23). Each row in the figure corresponds to different value of $<\Delta t>$. The first column shows the emission time distributions for positive and negative kaons. The second column presents the correlation functions for two different orientations of the vector of relative momentum with respect to the pair CMS velocity ($R_+(\mathbf{k}^*\mathbf{v} \geq 0)$ and $R_-(\mathbf{k}^*\mathbf{v} < 0)$). The third column displays the ratio of the correlation functions from the second column. Despite the small differences in the form of correlation functions, their ratio shows the clear effect changing its sign according to $<\Delta t>$ and thus according to the order of particle emission.

The same is presented in the Fig.24 but for the scale factor $\alpha = 3.0$. Here, the same value of the time shift has different relative meaning as the absolute values of the emission times are different. This leads to the narrowing of the effect.

The influence of the detector resolution is presented in the Fig. 25. As in the previous cases three detector configurations are considered. In case of the total detection chain: TPC+SSD+SVT the sequence of particle emission can be observed. In the cases without the TPC the effect is strongly affected by the resolution, what precludes practically from extraction of the physical information. Therefore the improvement of the resolution for the particles with the small value of p_t appeares to be highly desirable. Here we approach the limits of the detector possibilities in case of large space-time dimensions of the particle source.

6.6 Correlations of short-lived particles

Neutral kaon interferometry is possible in STAR due to the short-lived particle reconstruction capabilities of the vertex detectors. The original SVT simulations showed that, on average, 2.5 K_s^0 (2.5 pairs) can be reconstructed per event. With the reconstruction efficiency enhancement obtained due to the SSD addition, around 9 K_s^0 (more than 30 pairs) should be expected. This corresponds to a strong increase, by a factor of 10, of the pair detection rate and consequently a decrease, by the same magnitude, of the running time necessary to collect a K_s^0 pair sample statistically significant.

In fact the strong improvement of the Λ reconstruction efficiency obtained by the addition of the SSD opens the possibility of measuring Λ-pairs in an event. Before the inclusion of the SSD, the SVT efficiency leads to about 0.5 reconstructed Λ per event. SSD will enhance the Λ yield per event by about a factor five. The number of reconstructed Λ pairs is then comparable to the number of K_s^0-pairs.

7 Conclusion

We discussed possible effects giving rise to correlations of identical and non-identical particles at small relative velocities and demonstrated the ability of the STAR detector for determination of the space-time characteristics of particle production in heavy-ion collisions at RHIC.

We have shown that unlike-particle correlations, compared with those of identical particle, contain a principally new piece of information on the relative space-time asymmetries in particle emission, thus allowing, in particular, a measurement of the mean relative delays in particle emission at time scales as small as 10^{-23} s. To determine these asymmetries, the unlike-particle correlation functions R_+ and R_- have to be studied separately for positive and negative values of the projection of the relative momentum vector in pair c.m.s. on the pair velocity vector or, generally, - on any direction of interest. The results of simulations of a number of two-particle systems, using the event generator VENUS, adapted somewhat arbitrarily for RHIC conditions, and including the expected resolution of the STAR detector, demonstrated that the R_+/R_- ratio is sufficiently sensitive to the relative time delays of few fm/c.

The influence of the multi-boson effects on boson multiplicities, single-boson spectra and two-boson correlations, including an approximate scaling behavior of some of their characteristics with the phase-space density, has been demonstrated using the simple analytically solvable Gaussian model. Though these effects are hardly to be observable in typical events of heavy ion collisions at present and perhaps also in future heavy-ion experiments, they can clearly show up in some rare events or - in the regions of momentum space with a large pion phase-space density.

Correlations of short-lived particles can be measured at STAR due to the tracking capabilities of the vertex detectors. We expect, that the neutral kaon interferometry analysis will be performed in good, statistically significant conditions. A new possibility of measuring Λ pairs will be open due to the addition of SSD.

References

[1] G. Goldhaber et al., *Phys. Rev.* **120** (1960) 300.

[2] G.I. Kopylov, M.I. Podgoretsky, *Yad. Fiz.* **15** (1972) 392; G.I. Kopylov, *Phys. Lett.* **B50** (1974) 472;

[3] M.I. Podgoretsky, *Fiz. Elem. Chast. Atom. Yad.* **20** (1989) 628 (*Sov. J. Part. Nucl.* **20** (1989) 266).

[4] S.E. Koonin, *Phys. Lett.* **B70** (1977) 43.

[5] M. Gyulassy, S.K. Kauffmann, L.W. Wilson, *Phys. Rev.* **C20** (1979) 2267.

[6] R. Lednicky, V.L. Lyuboshitz, *Yad. Fiz.* **35** (1982) 1316 (*Sov. J. Nucl. Phys.* **35** (1982) 770); Proc. Int. Workshop on Particle Correlations and Interferometry in Nuclear Collisions, CORINNE 90, Nantes, France, 1990 (ed. D. Ardouin, World Scientific, 1990) p. 42; JINR report P2-546-92 (1992) 1; *Heavy Ion Physics* **3** (1996) 93.

[7] D.H. Boal, J.C. Shillcock, *Phys. Rev.* **C33** (1986) 549.

[8] R. Lednicky, V.L. Lyuboshitz, B. Erazmus, D. Nouais, *Phys. Lett.* **B373** (1996) 30; Report SUBATECH 94-20, Nantes 1994.

[9] V.G. Grishin, G.I. Kopylov, M.I. Podgoretsky, *Yad. Fiz.* **13** (1971) 1116.

[10] G.H. Thomas, *Phys. Rev.* **D15** (1977) 2636.

[11] P. Grassberger, *Nucl. Phys.* **B120** (1977) 231.

[12] B.V. Batyunya et al. (LUDMILA), *Yad. Fiz.* **27** (1978) 1556; R. Lednicky, Proc. III Europ. Symp. on Antinucl. Nucleon Int., Stockholm, 1976, *Wenner-Gren* **29** (1977) 477.

[13] B.V. Batyunya et al. (LUDMILA), *Czech. J. Phys.* **31** (1981) 475; R. Lednicky, JINR B2-3-11460, Dubna, 1978.

[14] R. Lednicky, M.I. Podgoretsky, JINR P2-12302, Dubna, 1979; JINR P2-82-327, Dubna, 1982.

[15] R. Lednicky, T.B. Progulova, *Z. Phys.* **C55** (1992) 295.

[16] M.G. Bowler, *Z. Phys.* **C29** (1985) 617.

[17] B. Andersson, W. Hofmann, *Phys. Lett.* **B169** (1986) 364.

[18] S. Pratt, *Phys. Rev. Lett.* **53** (1984) 1219; *Phys. Rev.* **D33** (1986) 1314; S. Pratt, T. Csorgo, J. Zimanyi, *Phys. Rev.* **C42** (1990) 2646.

[19] K. Kolehmainen, M. Gyulassy, *Phys. Lett.* **B130** (1986) 203.

[20] A.N. Makhlin, Yu.M. Sinyukov, *Yad. Fiz.* **46** (1987) 637; *Z. Phys.* **C39** (1988) 69; Yu.M. Sinyukov, *Nucl. Phys.* **A498** (1989) 151c.

[21] S.V.Akkelin, Yu.M. Sinyukov, *Phys. Lett.* **B356** (1995) 525.

[22] G. Bertsch, M. Gong, M. Tohyama, *Phys. Rev.* **C37** (1988) 1896.

[23] Y. Hama, S.S. Padula, *Phys. Rev.* **D37** (1988) 3237.

[24] U. Mayer, E. Schnedermann, U. Heinz, *Phys. Lett.* **B294** (1992) 69.

[25] B.R. Schlei, U. Ornik, M. Plumer, R.M. Weiner, *Phys. Lett.* **B293** (1992) 275; J. Bolz, U. Ornik, M. Plumer, B.R. Schlei, R.M. Weiner, *Phys. Lett.* **B300** (1993) 404.

[26] N.S. Amelin, R. Lednicky, *Heavy Ion Physics* **4** (1996) 241; SUBATECH 95-08, Nantes 1995, submitted to *Nucl. Phys.* **B**.

[27] B. Erazmus *et al.*, Internal Note ALICE 95-43, Geneve 1995; SUBATECH 98-03, Nantes 1998;

[28] B. Erazmus, N. Carjan, D. Ardouin, *Phys. Rev.* **C44** (1991) 2663; B. Erazmus, L. Martin, R. Lednicky, N. Carjan, *Phys. Rev.* **C49** (1994) 349.

[29] M.I. Podgoretsky, JINR Report **P2-85-240** (1985).

[30] W. Zajc, *Phys. Rev.* **D35** (1987) 3396.

[31] W.N. Zhang *et al.*, *Phys. Rev.* **C47** (1993) 795.

[32] S. Pratt, *Phys. Lett.* **B301** (1993) 159.

[33] S. Pratt, *Phys. Rev.* **C50** (1994) 469.

[34] G.F. Bertsch, *Phys. Rev. Lett.* **72** (1994) 2349.

[35] Yu.M. Sinyukov, B. Lorstad, *Z. Phys.* **C61** (1994) 587.

[36] J. Barrette *et al.*, *Phys. Rev. Lett.* **78** (1997) 2916.

[37] B. Jacak, Proc. Int. Workshop on Multiparticle Correlations and Nuclear Reactions, CORINNE II, Nantes, France, 1994 (ed. J. Aichelin and D. Ardouin, World Scientific, 1994) p. 3.

[38] M. Gazdzicki, *Nucl. Phys.* **A590** (1995) 197c.

[39] Yu.M. Sinyukov, B. Lorstad, V.A. Averchenkov, *Z. Phys.* **C49** (1991) 417.

[40] Proc. of "Quark Matter 93", *Nucl. Phys.* **A566** (1994).

[41] D.V. Anchishkin, W.A. Zajc, G.M. Zinovjev, *Ukrainian J. Phys.* **41** (1996) 363.

[42] K. Werner, *Phys. Rep.* **232** (1993) 87.

[43] Klaus Werner and Jörg Aichelin, *Phys. Rev.* **C52** (1995) 1584.

[44] Proposal for a Silicon Strip Detector for STAR (SSD), (1998)

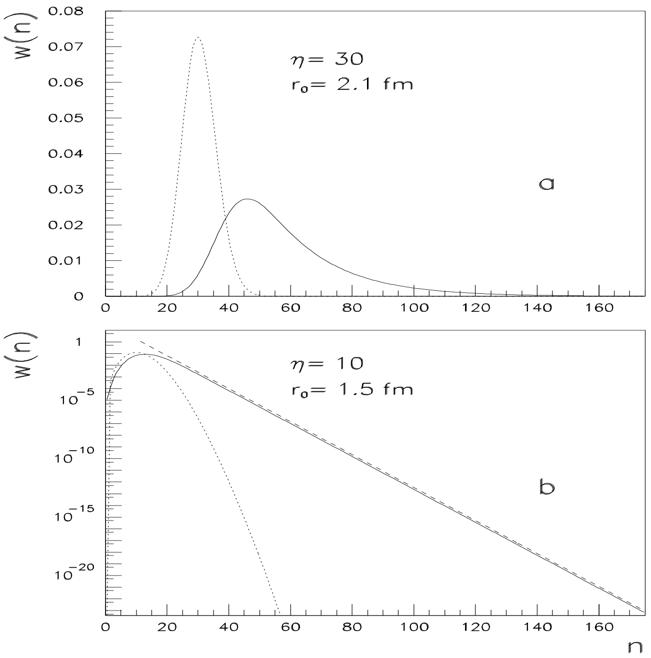

Figure 1: The multiplicity distribution of neutral pions for a) $\Delta = 0.25$ GeV/c, $r_0 = 2.1$ fm, $\eta = 30$ and b) $\Delta = 0.25$ GeV/c, $r_0 = 1.5$ fm, $\eta = 10$, where η is the mean multiplicity of the original Poissonian distributions (dotted curves).

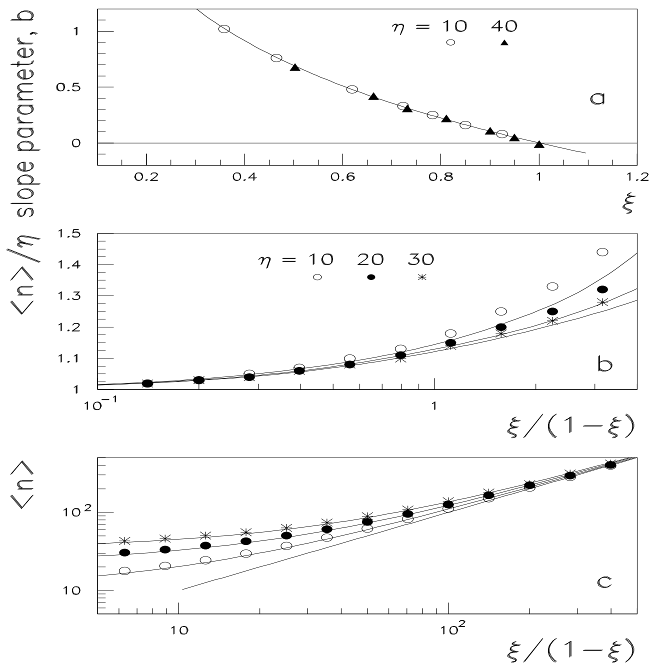

Figure 2: The slope parameter b of the exponential tail $c \cdot \exp(-b \cdot n)$ of the multiplicity distribution (a), the ratio of the mean multiplicity to the original Poissonian one (b) and the mean multiplicity (c) as functions of the density parameters $\xi = \eta/\beta$ and $\xi/(1-\xi)$; $\Delta = 0.25$ GeV/c. The curve in (a): $b = -\ln\xi$, the curves in (b), (c) are calculated according to the tailing approximation in Eq. (11), the line in (c): $\langle n\rangle = \xi/(1-\xi) \equiv \nu$.

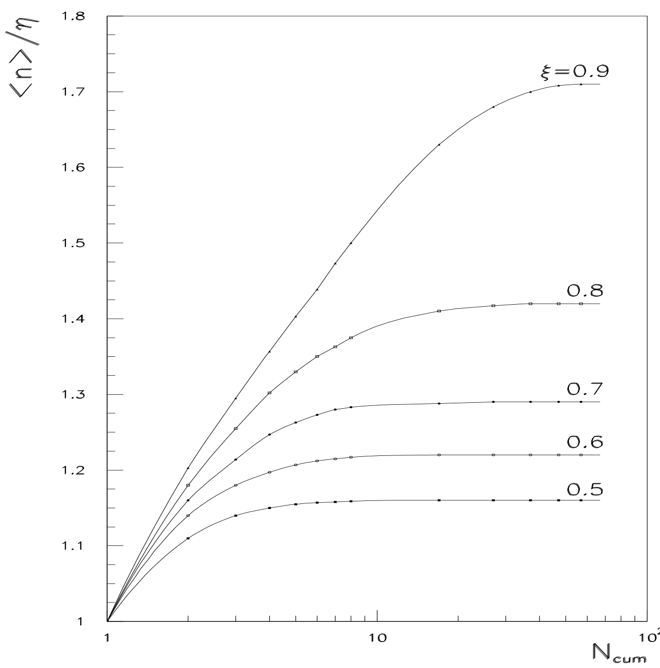

Figure 3: The ratio of the mean multiplicity to the original Poissonian one as a function of the number of the contributing cumulants for diffrent values of the density parameter ξ.

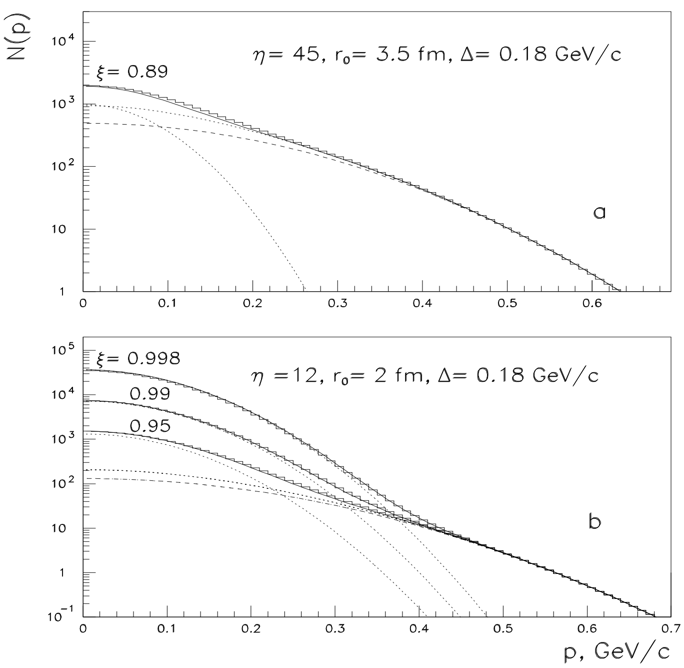

Figure 4: The inclusive single-particle spectra corresponding to the density parameters a) $\xi = 0.89$ and b) $\xi = 0.95$, 0.99 and 0.998 (the corresponding radius r_0 slightly varies near 2 fm). The full curves are calculated according to the tailing approximation (15), the dotted ones represent the contributions of the two (BE gas and BE condensate) terms in Eq. (15), the dashed curves, $\eta P(\mathbf{p})$, correspond to the rare gas limit.

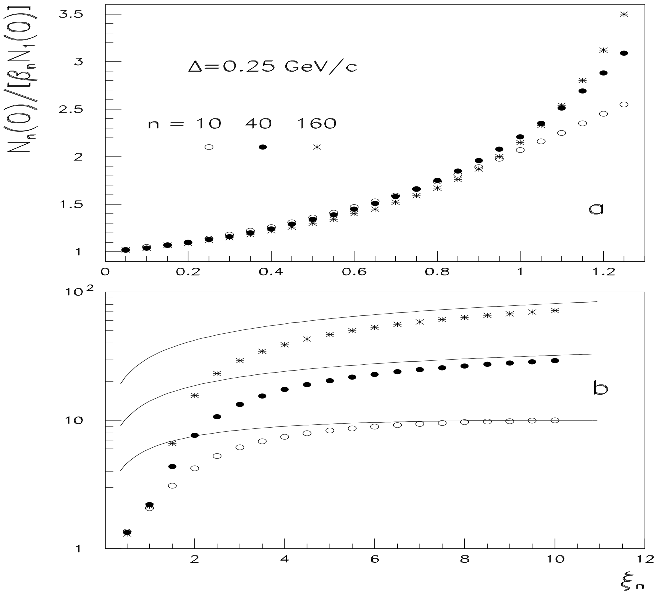

Figure 5: The ratios of the BE affected single-particle spectrum to the dominant large-$\mathbf{p}$ contribution $\beta_n N_1(\mathbf{p})$, $\beta_n = n\omega_{n-1}/\omega_n$, calculated at $\mathbf{p} = 0$ as functions of the density parameter $\xi_n = n/\beta$. The curves represent the large-ξ_n limit: $(2r_0\Delta)^{3/2}\xi_n \equiv [2(n/\xi_n)^{1/3} - 1]^{3/2}\xi_n$.

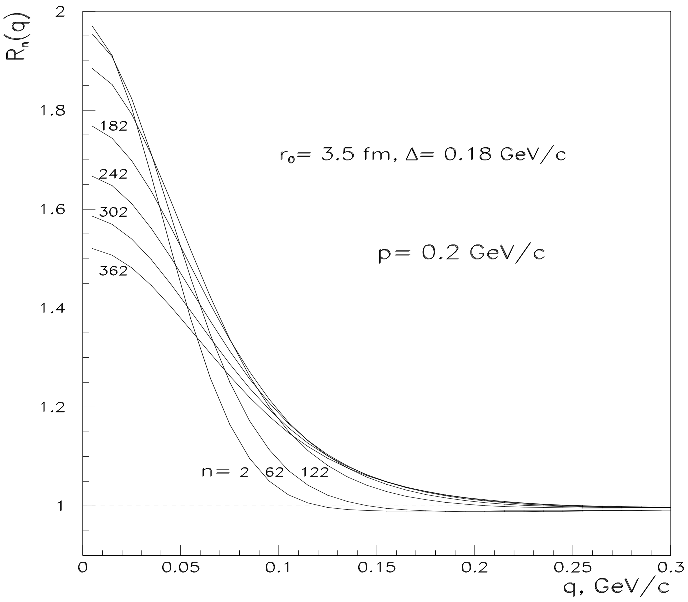

Figure 6: The two-pion correlation functions for the multiplicities increasing from $n = 2$ to 362 with a step of 60 (the corresponding density parameter ξ_n ranging from 0.04 to 7.2 with a step of 1.2). The higher is the multiplicity the lower is the intercept of the correlation function and the larger is its width.

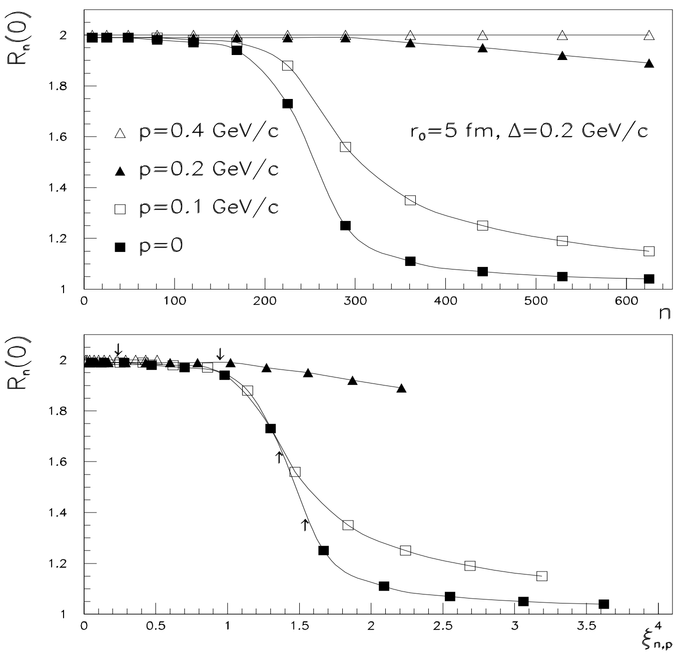

Figure 7: The intercept of the two-pion correlation functions as a function of the multiplicity n and the density parameter $\xi_{n,\mathbf{p}}$ for several values $p = 0,\ 0.1,\ 0.2$ and 0.4 GeV/c of the mean momentum of the two pions. The arrows on the interpolating curves indicate the intercept values corresponding to $\xi_n = 3\xi = 1.5$ ($n \approx 3\langle n\rangle$)

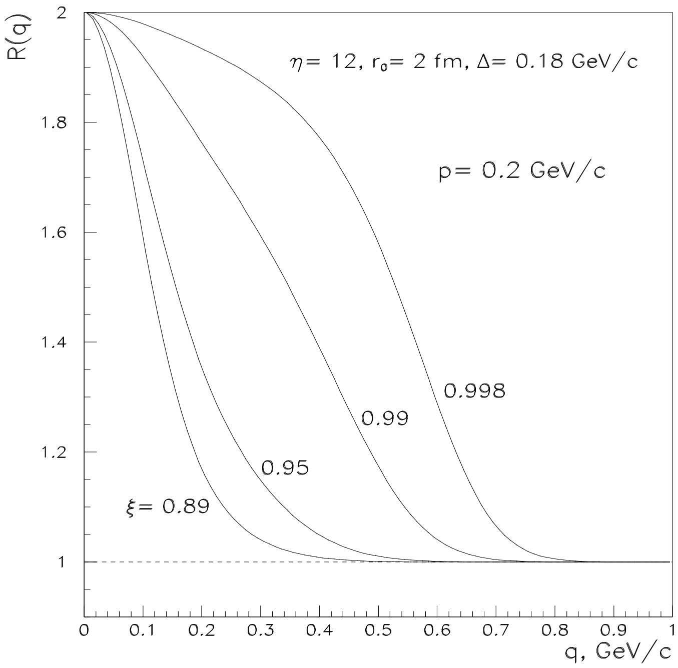

Figure 8: The inclusive two-pion correlation functions demonstrating the increase of the correlation width with the increasing density parameter ξ. The different ξ-values are achieved by slight variations of the radius r_0 around 2 fm.

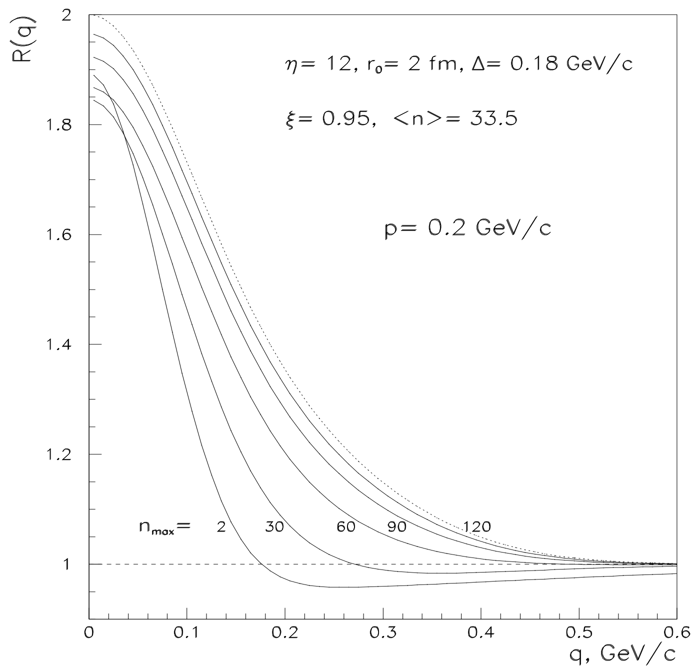

Figure 9: The semi-inclusive correlation functions including the pion multiplicities from 0 to n_{max} for different values of n_{max}. The dotted curve is the inclusive ($n_{max} \to \infty$) correlation function. The conditions are the same as in Fig. 8 for the density parameter $\xi = 0.95$.

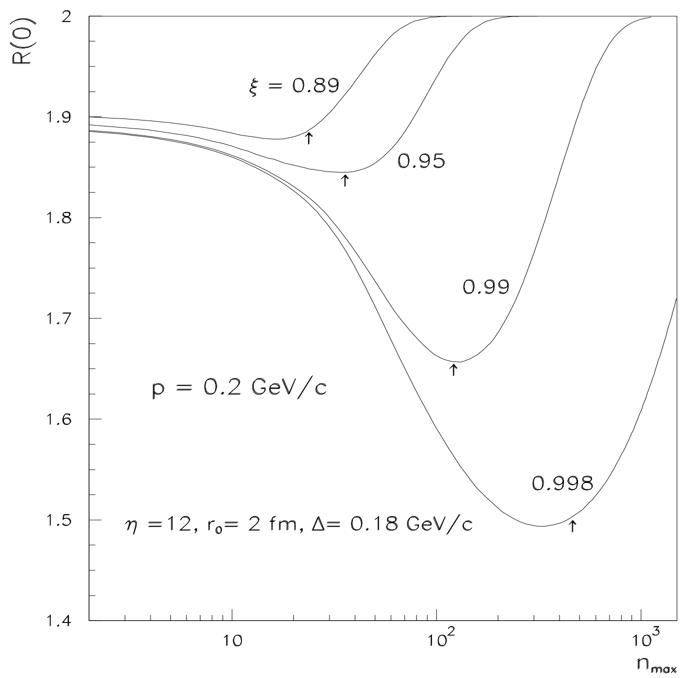

Figure 10: The intercepts of the semi-inclusive correlation function including the pion multiplicities from 0 to n_{max} as functions of n_{max} for different values of the density parameter $\xi = 0.89$, 0.95, 0.99 and 0.998; the arrows indicate the corresponding mean multiplicities $\langle n \rangle = 22.3$, 33.5, 113.7 and 433.8. The conditions are the same as in Fig. 8.

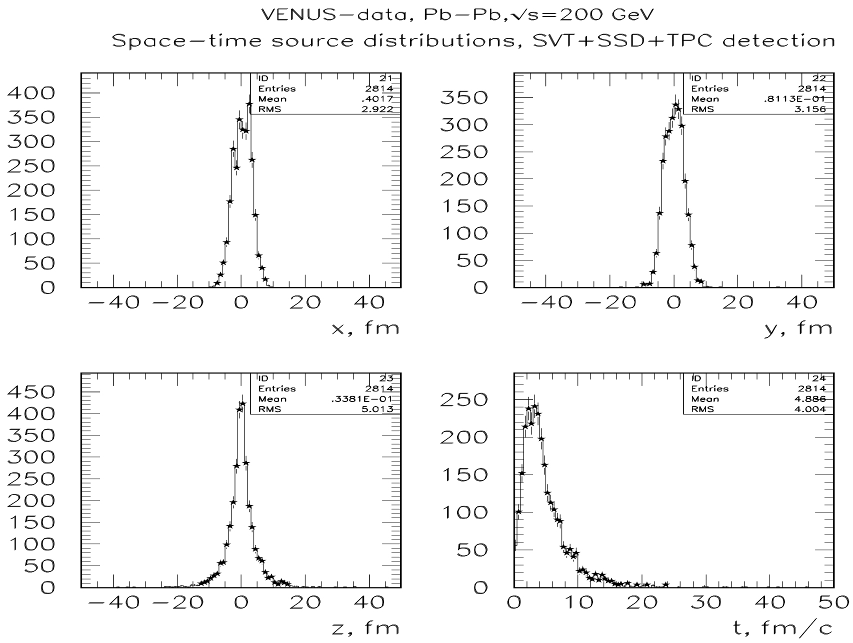

Figure 11: Space-time source distributions obtained from the simulated data (one VENUS event) for identical charged pions taking into account full (SVT+SSD+TPC) resolution, $(0.05 < P_t < 2.50) GeV/c$.

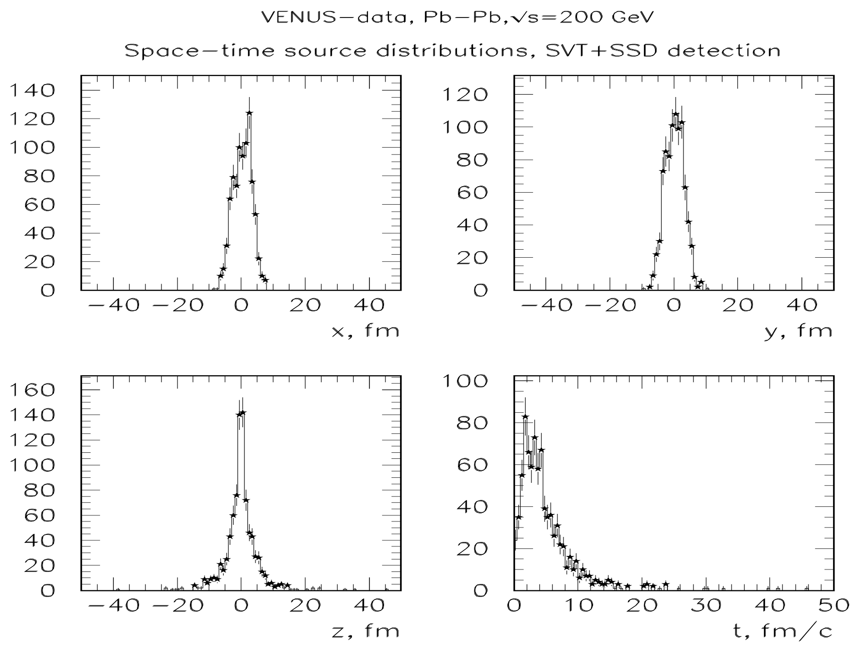

Figure 12: Space-time source distributions obtained from simulated data (one VENUS event) for identical charged pions with SVT+SSD resolution accounted for $p_t < 0.2 GeV/c$.

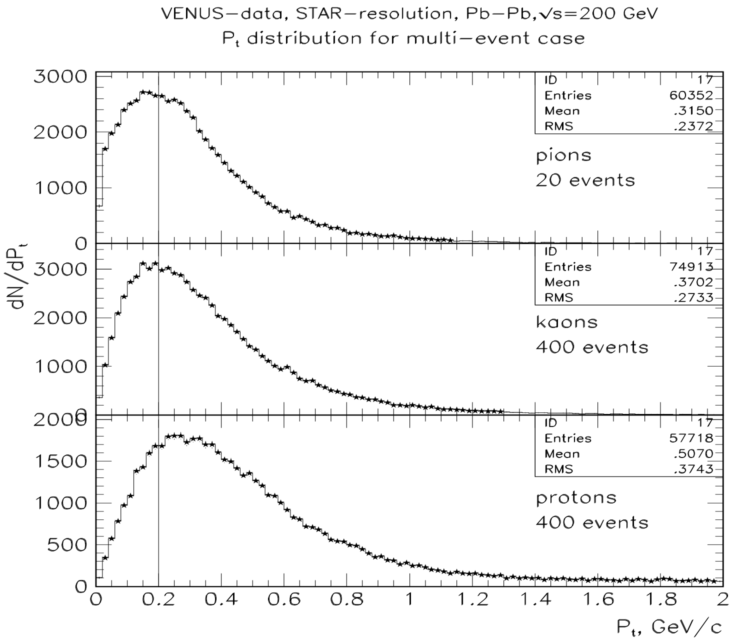

Figure 13: Transverse momentum (p_t) distributions for pions, kaons and protons.

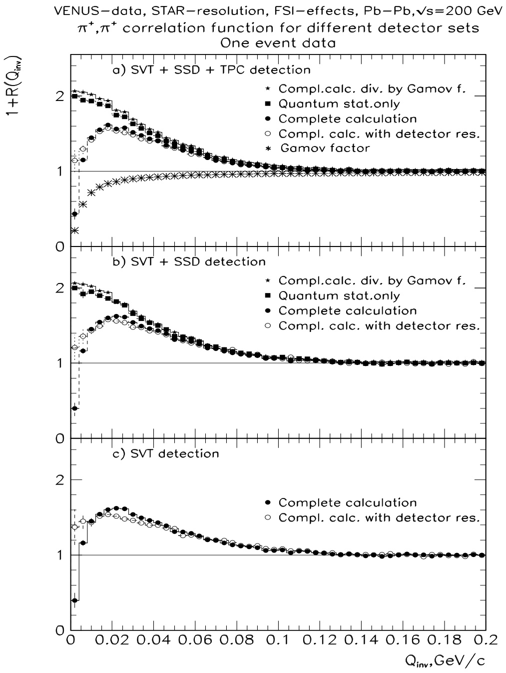

Figure 14: The simulated correlation functions for two identical charged pions without and with the experimental resolution accounted for. The simulations were done using VENUS model; the mean space-time coordinates of emission points are $\langle r \rangle = 5$ fm and $\langle t \rangle = 4$ fm/c in the reaction c.m.s. The Gamow corrected correlation function is compared with that including the effect of quantum statistics only.

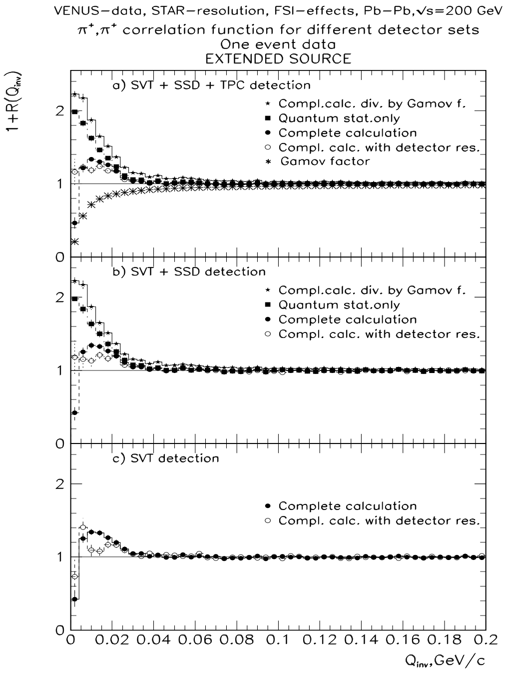

Figure 15: The same as Fig. 14, but with extended space-time emission characteristics (scale-factor = 3; $\langle r \rangle = 15$ fm, $\langle t \rangle = 15$ fm/c in the reaction c.m.s.).

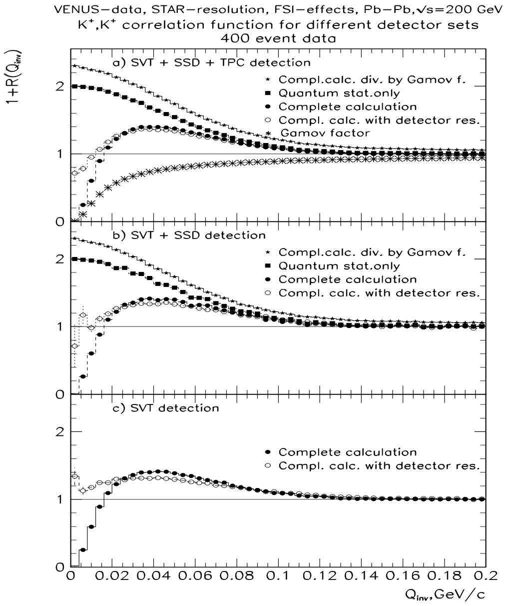

Figure 16: The simulated correlation functions for two identical charged kaons without and with the experimental resolution accounted for. The simulations were done using VENUS model; the mean space-time coordinates of emission points are $\langle r \rangle = 5$ fm and $\langle t \rangle = 4$ fm/c in the reaction c.m.s. The Gamow corrected correlation function is compared with that including the effect of quantum statistics only.

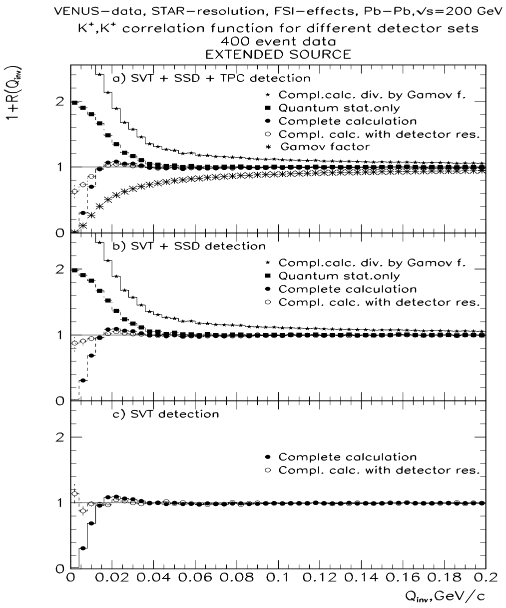

Figure 17: The same as Fig. 16, but with extended space-time emission characteristics (scale-factor = 3; $\langle r \rangle = 15$ fm, $\langle t \rangle = 15$ fm/c in the reaction c.m.s.).

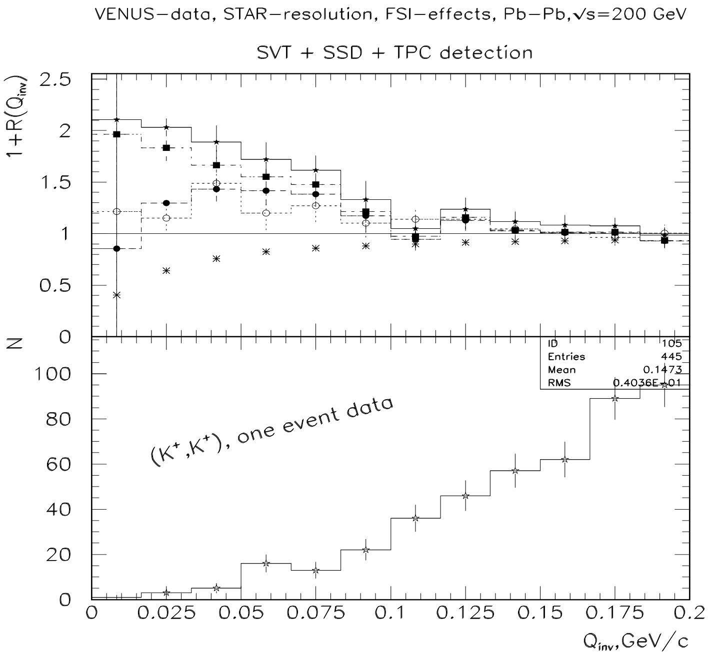

Figure 18: Simulated one-event correlation function for two identical charged kaons without (full circles) and with (open circles) the effect of the full (SVT+SSD+TPC) experimental resolution. Description the same as for previous figures.

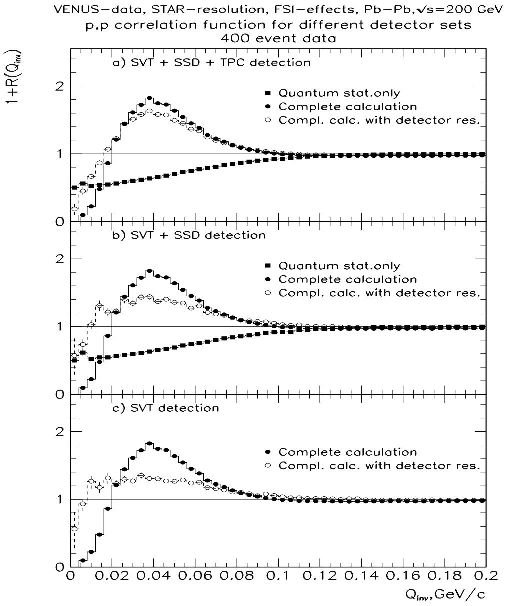

Figure 19: The simulated two-protons correlation functions without and with the experimental resolution accounted for. The simulations were done using VENUS model; the mean space-time coordinates of emission points are $\langle r \rangle = 5$ fm and $\langle t \rangle = 4$ fm/c in the reaction c.m.s.

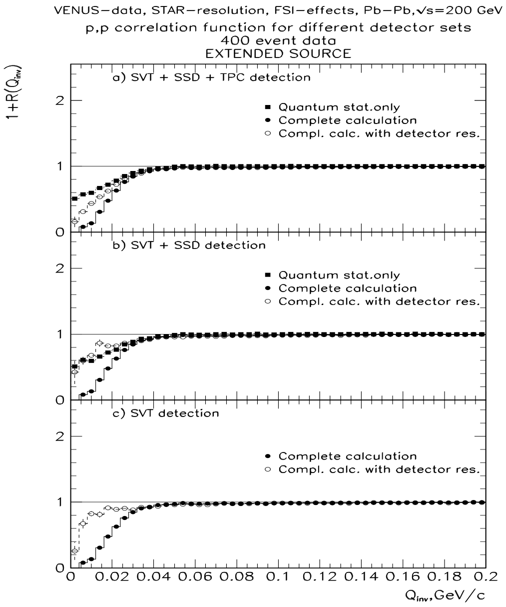

Figure 20: The same as Fig. 19, but with extended space-time emission characteristics (scale-factor = 3; $\langle r \rangle = 15$ fm, $\langle t \rangle = 15$ fm/c in the reaction c.m.s.).

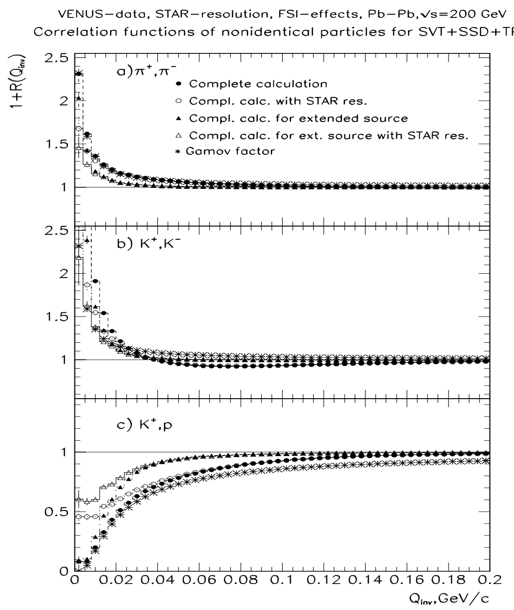

Figure 21: The simulated correlation functions for different pairs of particles with the experimental resolution accounted for. The simulations were done using VENUS model with two different space-time emission characteristics: taken directly from VENUS and extended by a factor of 3.

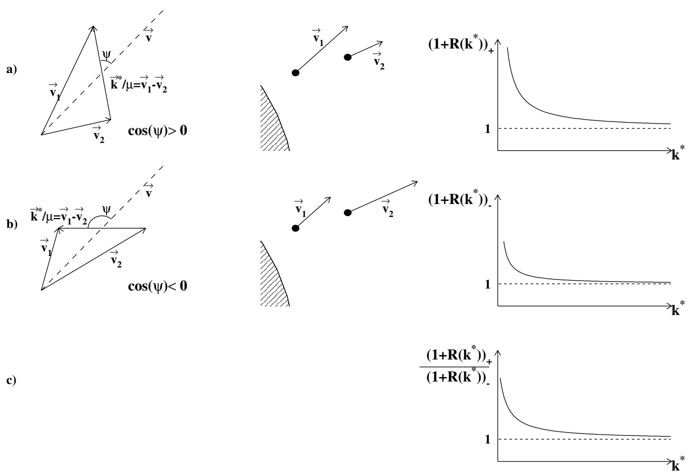

Figure 22: We can determine which sort of particles was produced earlier and which later by studying the correlation functions of two non-identical particles separately for the angles less and greater than 90° between the relative velocity $\mathbf{k}^*/\mu$ ($\mathbf{k}^* = \mathbf{p}_1^* = -\mathbf{p}_2^*$ and μ is the reduced mass of the two particles) and the total pair velocity $\mathbf{v}$.

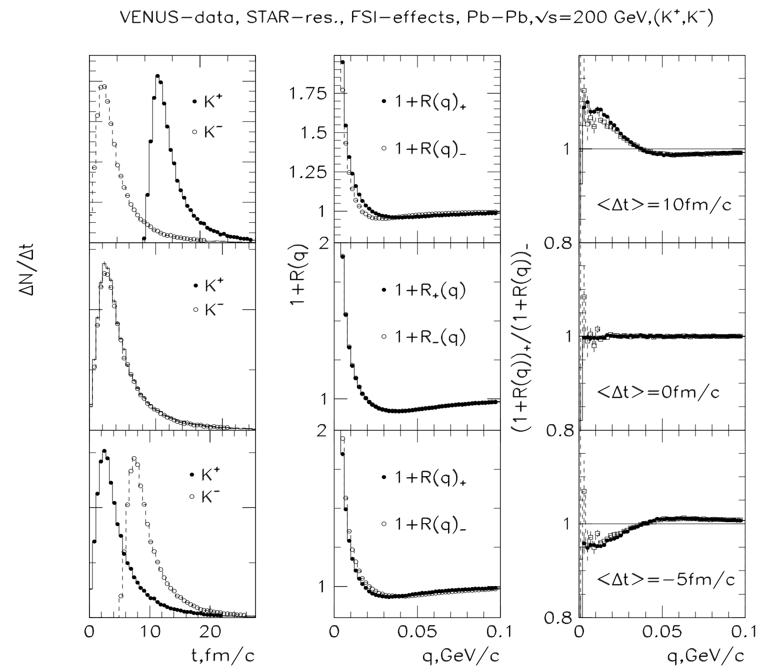

Figure 23: The distributions of the difference of the K^+ and K^- emission times $\Delta t = t_{K^+} - t_{K^-}$ simulated by VENUS with the shifts $\langle \Delta t \rangle$ =+10 and -5 fm/c introduced *ad hoc* and the corresponding correlation functions R_+ ($\mathbf{v} \cdot \mathbf{k}^* \geq 0$) and R_- ($\mathbf{v}\mathbf{k}^* < 0$) and their ratios calculated for K^+K^- pairs. The ratios distorted by the effect of experimental resolution are represented by open symbols.

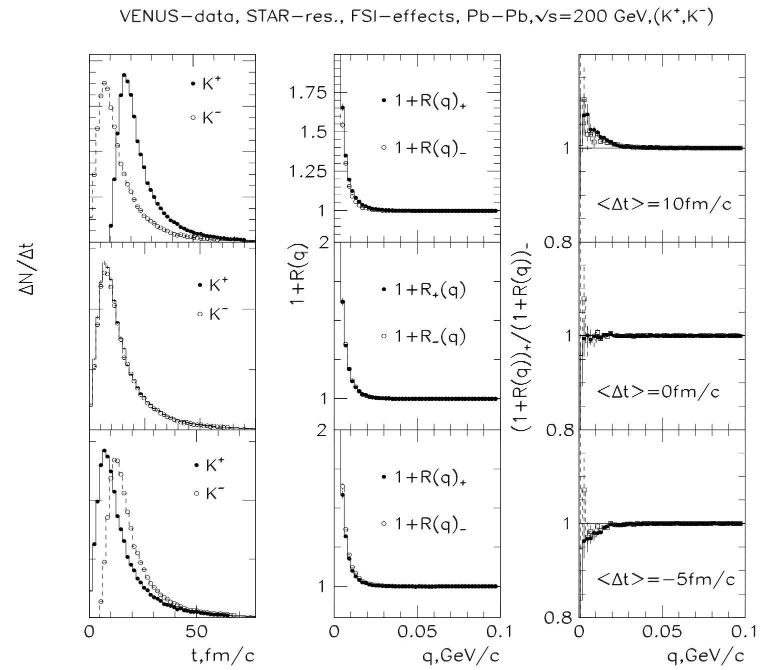

Figure 24: The same as Fig. 23, but for extended space-time emission characteristics (by factor of 3.)

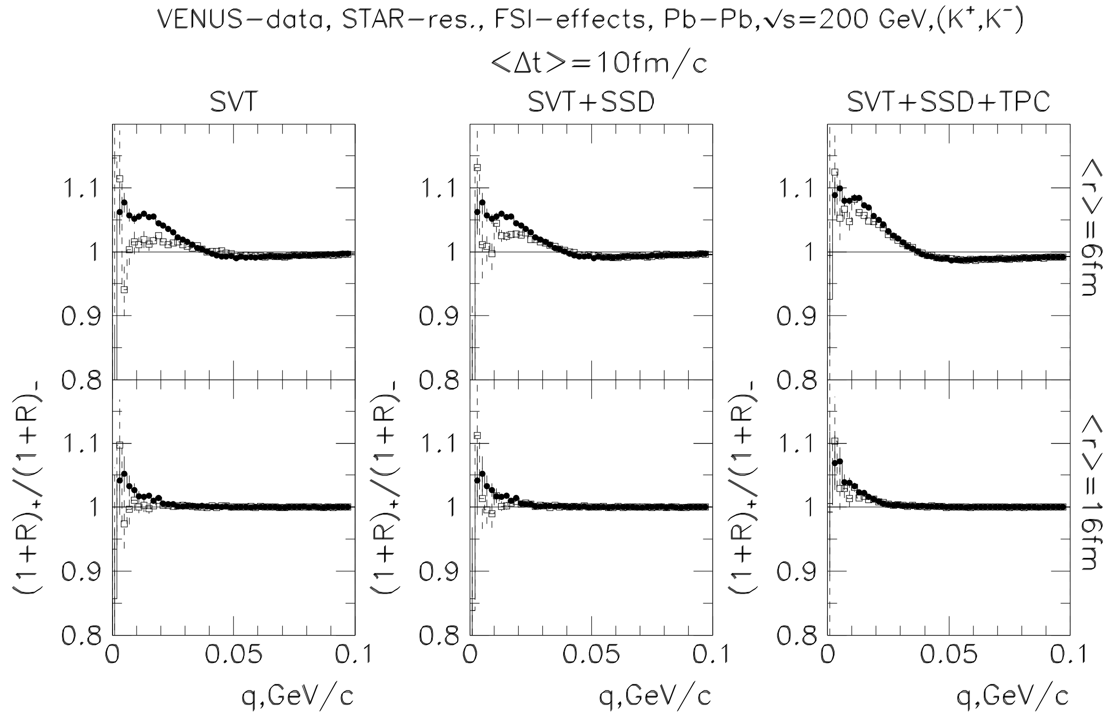

Figure 25: The same ratios R_+/R_- as in Fig. 23 calculated with $\langle \Delta t \rangle = +10$ fm/c, for different detector sets, taking into account (open symbols) and neglecting (full symbols) the effect of experimental resolution.